analytical chemistry

ARTICLE

pubs.acs.org/ac

Acid−Base Equilibria inside Amine-Functionalized Mesoporous Silica

Akira Yamaguchi,[*,†] Manato Namekawa,[‡] Toshio Kamijo,[‡,⊥] Tetsuji Itoh,[§] and Norio Teramae[*,‡]

[†]College of Science and Frontier Research Center for Applied Atomic Sciences, Ibaraki University, 2-1-1 Bunkyo, Mito, Ibaraki 310-8512, Japan

[‡]Department of Chemistry, Graduate School of Science, Tohoku University, Aoba-ku, Sendai 980-8578, Japan

[§]Research Center for Compact Chemical System, National Institute of Advanced Industrial Science and Technology (AIST), Nigatake 4-2-1, Miyagino-ku, Sendai 983-8551, Japan

Supporting Information

ABSTRACT: Acid−base equilibria and effective proton concentration inside a silica mesopore modified with a trimethyl ammonium (TMAP) layer were studied by steady-state fluorescence experiments. The mesoporous silica with a dense TMAP layer (1.4 molecules/nm^2) was prepared by a post grafting of *N*-trimethoxysilylpropyl-*N*,*N*,*N*-trimethylammonium at surfactant-templated mesoporous silica (diameter of silica framework =3.1 nm). The resulting TMAP-modified mesoporous silica strongly adsorbed of anionic fluorescence indicator dyes (8-hydroxypyrene-1,3,6-trisulfonate (pyranine), 8-aminopyrene-1,3,6-trisulfonate (APTS), 5,10,15,20-tetraphenyl-21H,23H-porphinetetrasulfonic acid disulfuric acid (TPPS), 2-naphthol-3,6-disulfonate (2NT)) and fluorescence excitation spectra of these dyes within TMAP-modified mesoporous silica were measured by varying the solution pH. The fluorescence experiments revealed that the acid−base equilibrium reactions of all pH indicator dyes within the TMAP-modified silica mesopore were quite different from those in bulk water. From the analysis of the acid−base equilibrium of pyranine, the following relationships between solution pH (pH_{bulk}) and the effective proton concentration inside the pore (pH_{pore}) were obtained: (1) shift of pH_{pore} was 1.8 ($\Delta pH_{pore} = 1.8$) for the pH_{bulk} change from 2.1 to 9.1 ($\Delta pH_{bulk} = 7.0$); (2) pH_{pore} was not simply proportional to pH_{bulk}; (3) the inside of the TMAP-modified silica mesopore was suggested to be in a weak acidic or neutral condition when pH_{bulk} was changed from 2.0 to 9.1. Since these relationships between pH_{bulk} and pH_{pore} could explain the acid−base equilibria of other pH indicator dyes (APTS, TPPS, 2NT), these relationships were inferred to describe the effective proton concentration inside the TMAP-modified silica mesopore.

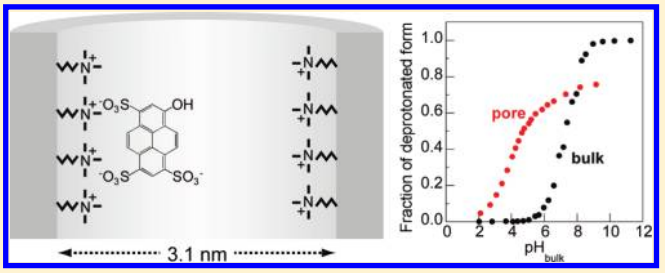

Recent progress in the fabrication of inorganic nanoporous materials allows use of their confined nanospace, surrounded by an inorganic framework, as a unique reaction field; applications have been made in the areas of catalyst, separation, sensor, and fuel cell.[1−10] In these applications, the efficiency and selectivity of the various chemical processes that occur inside the confined nanospace are commonly regulated by proton dissociation and transfer reactions. Clarification of the effective proton concentration and the acid−base equilibrium reactions inside the confined nanospace is important for promoting the science and technology of the nanoporous materials.

Several research groups have studied the acid−base equilibria of surface functional groups, such as surface hydroxyl, amino, and carboxyl groups, at the inner pore surface.[11−14] Typically, measurement approaches were based on electrochemical or adsorption isotherm measurements. For instance, electrochemical measurements were used to observe permeation behavior of a charged redox probe, such as $Fe(CN)_6^{3-}$ and $Ru(NH_3)_6^{3+}$, into a nanoporous film on a solid electrode,[11,12] and adsorption isotherms of a charged organic adsorbate in a nanoporous material were measured by a spectroscopic method.[13,14] These approaches rely on the electrostatic interaction or repulsion between a charged probe molecule and surface functional groups, and permeation or adsorption behavior of the charged probe molecule depending on solution pH is used to analyze the dissociation degree and apparent dissociation constant of the surface functional groups. For example, Newton et al.[12] reported the apparent pK_a of surface aminopropyl group within a nanoporous silica opal film on a Pt electrode as 5.7 from an analysis of solution pH dependency of voltammetric response of a redox probe. Rosenholm et al.[14] examined adsorption of benzylamine inside surfactant-templated mesoporous silica, and the adsorption isotherms of benzylamine were used to evaluate apparent pK_a of surface silanol and carboxyl groups.

In the studies of acid−base equilibria of surface functional groups by electrochemical or adsorption isotherm measurements, evaluation of these pK_a values was sometimes carried out by assuming that effective pH in the vicinity of the inner pore

Received: November 14, 2010
Accepted: March 6, 2011
Published: March 21, 2011

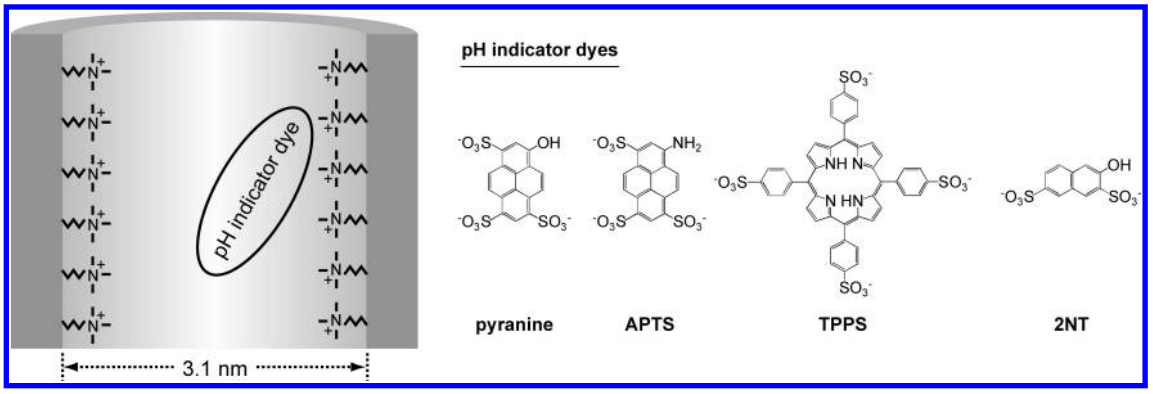

Figure 1. Scheme of TMAP-modified silica mesopore with a pH indicator dye adsorbed at the TMAP layer.

surface (pH_{pore}) was simply proportional to bulk solution pH (pH_{bulk}).[12,14] However, no direct evidence on the linear relationship between pH_{pore} and pH_{bulk} for an inorganic nanoporous system has been presented, and there is a possibility of a nonlinear relationship between pH_{pore} and pH_{bulk}. In addition, the acid−base equilibrium of an organic molecule inside the confined nanospace is unclear, although it affects adsorption and permeation behavior at the nanoporous material. The electrochemical and adsorption isotherm measurements cannot provide direct information on the dissociation state of a molecule inside the confined nanospace. Accordingly, further appropriate measurements and detailed analysis are necessary to discuss the acid−base equilibrium and effective pH inside the confined nanospace.

In this study, we examined acid−base equilibria of a series of fluorescent pH indicator dyes entrapped inside surfactant-templated mesoporous silica which is a well-known inorganic nanoporous material with an ordered and uniform pore structure. The most important advantage of the use of fluorescent pH indicator dyes is that their fluorescence spectra provide direct information on the molar ratio of all chemical forms, i.e., dissociated, neutral, and protonated forms of the pH indicator dyes.[15] The molar ratio of each form can be used to estimate effective proton concentration in the vicinity of a pH indicator dye when the Henderson−Hasselbalch equation describes the acid−base equilibrium of the pH indicator dye entrapped inside the silica mesopore. Various pH indicator dyes have been used to study acid−base equilibrium reactions for restricted environments such as a micelle surface,[16,17] reversed micelle cavity,[15,18,19] and polymer cavity.[20,21] On the other hand, our study is the first to use fluorescent pH indicator dyes for the study of acid−base equilibria and effective pH inside inorganic nanoporous materials.

To study the acid−base equilibria of fluorescent pH indicator dyes within mesoporous silica, the amount of the respective pH indicator dye within mesoporous silica must be kept constant during the fluorescent measurements. We modified the inner pore surface of mesoporous silica by trimethyl aminopropyl (TMAP) groups to get strong adsorption of an anionic fluorescent pH indicator at the surface of the positively charged TMAP layer by electrostatic interaction. Figure 1 shows the scheme of the TMAP-modified silica mesopore, together with chemical structures of the anionic fluorescent pH indicator dyes. In the present study, mesoporous silica (silica framework diameter, 3.1 nm) was formed within a porous anodic alumina membrane[22,23] and this hybrid mesoporous membrane (HMM) was used as a mesoporous silica specimen. After modification with TMAP groups, a fluorescent pH indicator dye was adsorbed within the TMAP-modified HMM (TMAP-HMM), and fluorescence excitation spectra of the fluorescence pH indicator dye were measured while varying solution pH. The fluorescence pH indicator dyes used show two distinct excitation bands corresponding to protonated and deprotonated forms.[15,24−28] From our analysis of excitation band intensities for the two forms, we considered the acid−base equilibria of the pH indicators and the effective pH inside the TMAP-modified silica mesopore.

EXPERIMENTAL SECTION

Chemicals. Cetyltrimetylammonium bromide (CTAB) was purchased from Tokyo Chemical Industry Co., Ltd. (Tokyo, Japan). *N*-trimethoxysilylpropyl-*N*,*N*,*N*-trimethylammonium chloride (TMSPA, 50 wt % in methanol) was purchased from AZmax Co., Ltd. (Chiba, Japan). Other chemicals and solvents used for the preparation of the TMAP-HMM were purchased from Wako Pure Chemical Industries Ltd. (Osaka, Japan). 8-Hydroxypyrene-1,3,6-trisulfonic acid trisodium salt (pyranine) was purchased from Sigma-Aldrich Japan (Tokyo, Japan). 5,10,15,20-Tetraphenyl-21H,23H-porphinetetrasulfonic acid disulfuric acid tetrahydrate (TPPS) was purchased from Dojindo Laboratories (Kumamoto, Japan). 8-Aminopyrene-1,3,6-trisulfonate (APTS), 2-naphthol-3,6-disulfonic acid disodium salt (2NT), and other chemicals used for the fluorescence measurements were purchased from Wako Pure Chemical Industries Ltd. All chemicals were used as-received. Milli-Q water was used for all experiments.

Preparation and Characterization of TMAP-HMM. The HMM was prepared according to the literature.[22] In brief, an acidic precursor solution containing CTAB and tetraethoxysilane (TEOS) was used to form surfactant-templated mesoporous silica within columnar alumina pores in a porous anodic alumina membrane by an aspiration method. After calcination to remove the template surfactant,[29] the calcined membrane was immersed in a mixture of 1,4-dioxane (29.7 mL) and TMSPA (0.3 mL) and heated under reflux for 12 h at 102 °C. After refluxing, the TMAP-HMM was rinsed with acetone and water three times each. The pore structure of TMAP-HMM and the surface TMAP layer were characterized by nitrogen adsorption and desorption isotherm, X-ray diffraction (XRD), ^{29}Si CP(Cross Polarization)/MAS(Magic Angle sample Spinning) NMR, and elemental analysis measurements. The experimental details of these measurements are described in Supporting Information.

Fluorescence Measurements. The TMAP-HMM was immersed in 10 mL of an aqueous solution containing 1 mM of a

Table 1. Dissociation Constants in Bulk Water (pK_{bulk}) and Amounts of pH Indicators inside Pores

system	pK_{bulk}[a]	amount of pH indicator[b]/mmol g^{-1}	$A^c/10^2$ nm^2 molecule^{-1}
pyranine	7.4	0.26	3.6
APTS	3.1	0.051	18
TPPS	4.8[d]	0.2	4.6
2NT	9.4	0.14	6.8

[a] Values derived from the excitation spectra in bulk water. [b] Values derived from the adsorption profiles of pH indicator dyes. [c] Space occupied by a single pH indicator molecule inside the TMAP-modified silica pore. [d] $(pK_1 \cdot pK_2)^{1/2}$.

Table 2. Structural Parameters of HMM and TMAP-HMM

system	BET surface area[a]/m^2 g^{-1}	BJH pore diameter[a]/nm	nitrogen content[b]/%	d_{TMAP}[c]/ molecules nm^{-2}
HMM	56	3.1		
TMAP-HMM	32	2.3	0.2	1.4

[a] Values derived from the nitrogen adsorption and desorption isotherms of HMM and TMAP-HMM. [b] Results of elemental analysis. [c] Surface density of TMAP groups.

pH indicator dye for adsorption of the dye within TMAP-HMM. The adsorption process was monitored by observing time-course absorption spectra of the solution phase according to the literature.[30] The concentrations of pH indicator dyes were estimated from the absorption spectra of the solution phase (Figure S1, Supporting Information), and those values are listed in Table 1. After adsorption of the pH indicator dye, the membrane was rinsed with Milli-Q water carefully and was fixed on a Teflon specimen holder in a quartz cell (1 cm ×1 cm). Then, the quartz cell was filled with water for the measurements. The pH of the measurement solution with the dye-absorbed TMAP-HMM specimen was adjusted using solutions of HCl and NaOH. Steady-state fluorescence spectra of pyranine were measured with a JASCO FP-6500 spectrofluorophotometer. The fluorescence measurements were done at 25 °C.

RESULTS AND DISCUSSION

Structural Characterization of TMAP-HMM. The structural parameters of mesoporous silica phase in HMM deduced from nitrogen adsorption isotherms are summarized in Table 2. Nitrogen adsorption isotherms and pore size distribution curves of TMAP-HMM and HMM are shown in Figure S2, Supporting Information. The pore diameter for HMM is estimated as 3.1 nm, which agrees with CTAB-templated mesoporous silica formed inside columnar alumina pores.[22,29] The BET surface area and pore diameter of TMAP-HMM are smaller than those of HMM, which is ascribed to the formation of the TMAP layer on the inner surface of the silica mesopore.

The X-ray diffraction (XRD) pattern of HMM suggested a quasi-hexagonal pore arrangement for the mesoporous silica phase in HMM (Figure S3a, Supporting Information). This pore arrangement agrees with a transmission electron microscopy images in our previous study; the CTAB-templated mesoporous silica formed inside columnar alumina pores was an assembly

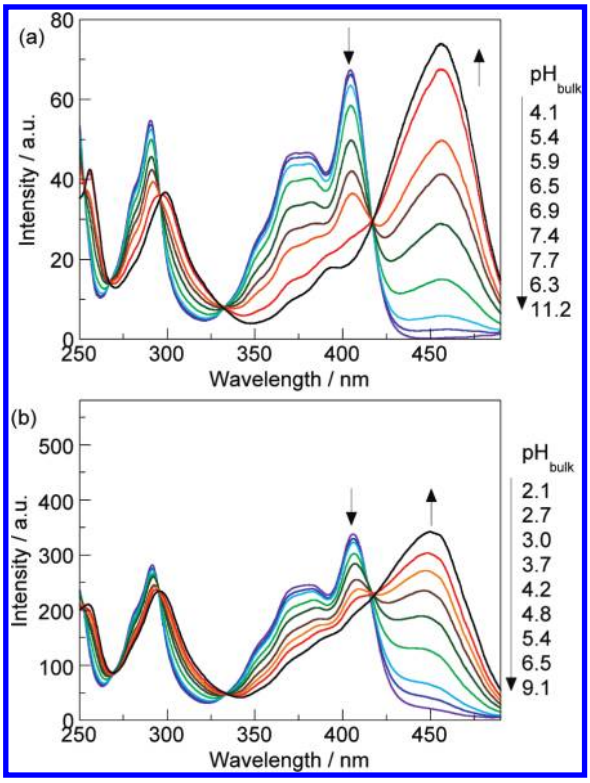

Figure 2. Fluorescence excitation spectra (λ_{em} = 510 nm) of pyranine (a) in bulk water and (b) within TMAP-HMM.

of straight silica nanochannels and the channel direction was predominantly oriented along the wall of the columnar alumina pore.[22] The intensity and shape of the XRD pattern of the TMAP-HMM are almost the same as those for the HMM (Figure S3aSupporting Information), indicating that the pore structure is not broken during the TMAP modification. In the ^{29}Si CP/MAS NMR spectrum of TMAP-HMM (Figure S3(b), Supporting Information), there are resonance peaks attributed to the T^3 and T^2 (T^m = $RSi(OSi)_mOH_{3-m}$) silicon sites and the resonance peak attributed to T^1 silicon site is negligibly small. This result indicates that the TMAP groups are immobilized on the inner silica wall in bi- and tridentate forms.[31−33] Two to three of the methoxy groups of TMSPA would be hydrolyzed and condensed with the surface silanols or with other hydrolyzed TMSPA.[32,33]

The nitrogen and carbon contents derived from the elemental analysis were used for the estimation of the surface density of the TMAP groups immobilized on the inner pore surface. The details of the estimation procedures were described in our previous paper,[34] and the estimated value is 1.4 molecules/nm^2. The surface density of the aminopropyl groups has been reported as 2 to 3 molecules/nm^2 at the maximum density.[35,36] On the other hand, the maximum surface density of TMAP groups can be considered as smaller than that of aminopropyl groups due to the steric and electrostatic repulsion of the quaternary ammonium headgroup of the TMAP. Accordingly, the surface density of 1.4 molecules/nm^2 suggests formation of a dense TMAP layer at the inner surface of the silica mesopore.

The density of surface silanols for surfactant-templated mesoporous silica has been believed to be lower than that for usual amorphous silica because well-ordered mesoporous silica has a highly condensed surface with less SiOH groups.[37,38] For CTAB-templated mesoporous silica, the density of surface silanols has

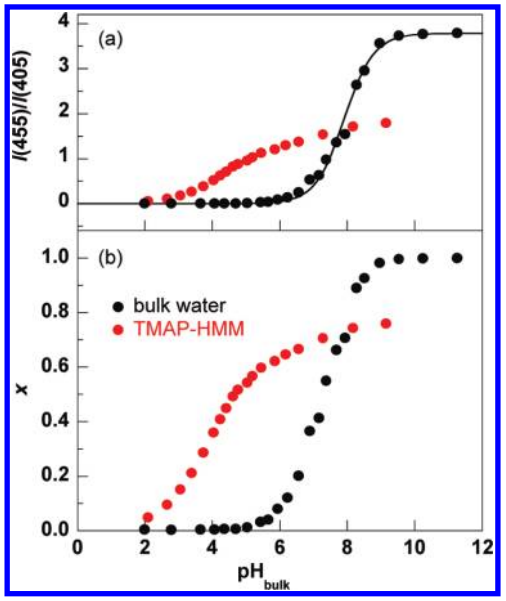

Figure 3. (a) Excitation band intensity ratio ($I(455)/I(405)$) of pyranine in bulk water and within TMAP-HMM as a function of solution pH (pH_{bulk}). (b) Estimated fraction (x) of deprotonated form of pyranine in bulk water and within TMAP-HMM as a function of pH_{bulk}. The solid curve in (a) denotes the best fit to eq 2.

been reported to be around 2.5−3.0/nm^2.[37,38] When the density (1.4 groups/nm^2) and the forms (bidentate and tridentate) of the surface TMAP groups are considered, the amount of residual surface silanols would not be so much. The net surface charge of the inner silica wall with the TMAP groups is an important factor to analyze the acid−base equilibrium reaction of pyranine within the TMAP-HMM. The immobilization of the dense TMAP groups suggests that the net surface charge is mainly governed by the positively charged headgroup of TMAP. This suggestion in the net surface charge is also supported by the fact of strong adsorption of pyranine discussed later.

Acid−Base Equilibrium of Pyranine. In the fluorescence excitation spectra of pyranine in bulk water as a function of solution pH (pH_{bulk}), isoemissive points can be recognized at 417, 333, 296, and 252 nm (Figure 2a). The existence of an isoemissive point suggests that the acid−base equilibrium at the hydroxyl group of pyranine in bulk water is described as follows:[15,24]

$$PyOH \rightleftharpoons PyO^- + H^+ \qquad (1)$$

where PyOH and PyO^- represent the protonated and deprotonated species of pyranine, respectively. As shown in Figure 2a, the intensities of the structured bands at 405 and 375 nm decrease and that of the band at 455 nm increases, as the pH_{bulk} value increases from 4.1 to 11.2. The bands at 405 and 375 nm can be ascribed to PyOH, and the band at 455 nm, to PyO^-.[15,24] The peak intensity ratio of these bands represents the fraction (x) of PyO^- form. The fluorescence intensity ratio at the 450 and 405 nm bands, $I(450)/I(405)$, was plotted as a function of pH (Figure 3a) to estimate x.

On the basis of Henderson−Hasselbalch equation, the relationship between the fluorescence intensity ratio and the fraction x can be expressed as

$$\frac{I(450)}{I(405)} = \frac{1}{\beta_1 10^{pK_{bulk} - pH_{bulk}} + \beta_2} \qquad (2)$$

where $\beta_1 = \beta_{PyOH}(\tilde{45})/\beta_{PyO-}(\tilde{45})$ and $\beta_2 = \beta_{PyO-}(\tilde{45})/\beta_{PyO-}(\tilde{45})$. $\beta_{PyO-}(\lambda)$ and $\beta_{PyOH}(\lambda)$ are fluorescence emission efficiencies of PyO^- and PyOH forms of pyranine at the designated wavelength of λ. The details in the development of eq 2 are described in Supporting Information. The value of pK_{bulk} was determined by the least-squares fitting of eq 2 to the observed pH dependence of the excitation band intensity ratio, $I(450)/I(405)$. The solid curve in Figure 3a represents the best fitting result with pK_{bulk} 7.4 of pyranine in bulk water. The fractions x, calculated by substituting pK_{bulk} of 7.4 into the Henderson−Hasselbalch equation, are shown in Figure 3b. It should be noted that pK_{bulk} and x obtained from the analysis of fluorescence data are almost the same as those obtained from an analysis of absorption spectra of pyranine in bulk water (Figure S4, Supporting Information), suggesting that the fractions shown in Figure 3b represent the fractions of PyO^- at the ground state.

In the fluorescence excitation spectra of pyranine within TMAP-HMM, isoemissive points can be also recognized at 417, 333, 295, and 252 nm when pH_{bulk} is below 9.1 (Figure 3b). The existence of an isoemissive point suggests that the amount of pyranine within TMAP-HMM is constant during the fluorescence measurements and that the acid−base equilibrium for the hydroxyl group of pyranine is maintained inside the TMAP-modified silica mesopore. On the other hand, the fluorescence intensity decrease occurs at higher pH_{bulk} than 9.1. This fluorescence intensity decrease is due to elution of pyranine from the TMAP-HMM accompanied by hydrolysis of the silica framework. When pH_{bulk} was below 2, it was difficult to obtain reliable fluorescence excitation spectra due to decomposition of the silica framework or removal of the surface TMAP groups at the high HCl concentration. Therefore, fluorescence spectra obtained at pH_{bulk} from 2.1 to 9.1 were used to estimate the fraction of PyO^-.

In the fluorescence excitation spectrum of pyranine within TMAP-HMM at pH_{bulk} 2.1, not only a structured band at 405 and 375 nm but also a band at 450 nm can be recognized (Figure 2b). The fluorescence excitation spectrum obtained at pH_{bulk} 9.1 has a strong band at 450 nm with small structured bands at 405 and 375 nm (Figure 2b). These spectra indicate the coexistence of PyO^- and PyOH forms within TMAP-HMM in the pH_{bulk} range from 2.1 to 9.1. It was difficult to obtain fluorescence excitation spectra of pure PyO^- and PyOH forms of pyranine in the present TMAP-HMM system because of its decomposition at high and low pH_{bulk} conditions. In the present study, therefore, β_1 and β_2 values obtained for the bulk water system were used to estimate the fraction of PyO^- form for the TMAP-HMM system using eq 2. As shown in Figure 2a,b, the peak wavelength of PyO^- form for the TMAP-HMM system is blue-shifted by 5 nm compared to that for bulk water, but the difference in fluorescence intensities at 450 and 455 nm is small (ca. 3%) due to the broad peak width. Accordingly, the difference of the peak wavelengths is not a critical problem for estimation of the fraction of PyO^- form.

The estimated fractions for bulk water and TMAP-HMM systems are shown in Figure 3b. The deprotonation of pyranine within TMAP-HMM takes place clearly at low pH_{bulk} conditions whereas the pyranine in bulk water undergoes hardly any deprotonation. On the other hand, the fraction of PyO^- form in TMAP-HMM is smaller than that for bulk water when pH_{bulk} is above 8.2. The increase in the fraction of PyO^- form can be recognized in a wide pH_{bulk} range (2.1 to 9.1). These

deprotonation behaviors of pyranine within TMAP-HMM are quite different from those in bulk water.

Effective pH inside TMAP-Modified Silica Mesopore. According to the studies on acid−base equilibria of pH indicators in various micellar systems,[16,17] the relationship between the fraction of PyO^- form, x, and pH_{pore} can be simply expressed as:

$$pK_{bulk} + \alpha = pH_{pore} - \log\left(\frac{x}{1-x}\right) \quad (3)$$

where pK_{bulk} is the dissociation constant of pyranine in bulk water and α represents an apparent shift value of the dissociation constant. The value of α of pyranine is affected by ionic strength, dielectric constant, and electrostatic potential at the surface of the TMAP layer.[16,17] Among them, the effect of ionic strength on the dissociation constant of pyranine would be negligible because the pK_{bulk} values of pyranine for bulk water with and without 4.5 M NaCl were almost the same. The α in the TMAP-HMM system most likely depends on the dielectric constant and electrostatic potential in the vicinity of the TMAP layer at the inner silica wall.

In TMAP-HMM, pyranine is located at the surface of the TMAP layer due to the electrostatic interaction between the positively charged TMAP head groups and three negatively charged sulfonate groups of pyranine; this is supported by the fact that hardly any desorption of pyranine adsorbed within TMAP-HMM occurred, whereas hydroxypyrene without sulfonate groups easily desorbed from TMAP-HMM. The net surface charge of the inner silica wall is positive and would not be influenced by the change in pH_{bulk} due to the presence of the dense TMAP in its bidentate and tridentate forms. Even if a small fraction of residual surface silanols is present after immobilization of TMAP, it can be considered that their deprotonations do not cause significant change in the net surface charge; this is also supported by the fact of the hardly any deprotonations of pyranine. If the net surface charge is perturbed by the deprotonaiton of the residual surface silanols, pyranine adsorbed by the electrostatic interaction will desorb. Accordingly, it can be considered that the electrostatic potential and the dielectric constant in the vicinity of pyranine within TMAP-HMM are independent of pH_{bulk} and the value of α for pyranine within TMAP-HMM is constant in the pH_{bulk} range from 2.1 to 9.1. This consideration means that the pH_{bulk}-dependent deprotonation behavior of pyranine within TMAP-HMM shown in Figure 3b can be analyzed using eq 3 with a constant α value in order to evaluate pH_{pore}.

Since pyranine is located at the surface of the dense TMAP layer, it is reasonably assumed that α in the TMAP-HMM system is close to that found for the surface of cationic micelle surfaces composed of cationic surfactants with a quaternary ammonium headgroup. Among various cationic micelle systems, α values for several pH indicators were reported in the range of 0 to −2.[16,17] It is difficult to estimate α only by fluorescent experiments with a pH indicator dye when proton concentration is unknown.[35] Therefore, pH_{pore} values at various pH_{bulk} were evaluated by substituting the fraction of PyO^- form shown in Figure 3b and α assumed as 0 or −2 in eq 3.

Figure 4 shows the relationship between pH_{pore} and pH_{bulk}. From this figure, several significant features of pH_{pore} dependency on pH_{bulk} are recognized. One is that the shift of pH_{pore} caused by the change in pH_{bulk} is small; the shift of pH_{pore} is 1.8 (ΔpH_{pore} = 1.8) for the pH_{bulk} change from 2.1 to 9.1 (ΔpH_{bulk} = 7). In addition, a nonlinear relationship with an inflection point at around pH_{bulk} = 4.7 is recognized between the increase in pH_{pore}

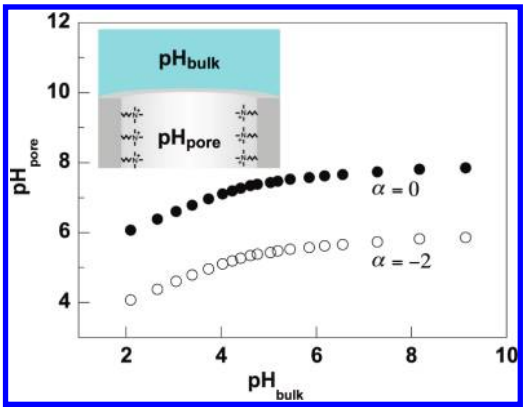

Figure 4. Relationship between pH_{pore} and pH_{bulk}. The values of pH_{pore} are evaluated from eq 3 for different α values (0 and −2).

and pH_{bulk}. Since these features are independent of α, it can be inferred that the small ΔpH_{pore} and the nonlinear relationship are intrinsic features of pH_{pore} vs pH_{bulk} in the TMAP-HMM system. The absolute value of pH_{pore} depends on α, and the shifts of pH_{pore} for the change in pH_{bulk} from 2.1 to 9.1 are 6.1 to 7.9 (α = 0) and 4.1 to 5.9 (α = −2). Although determination of absolute pH_{pore} is difficult due to uncertainty of α, by assuming that α in the TMAP-HMM system is close to that in cationic micelle surfaces, it can be said that the inside of the TMAP-modified silica mesopore is in the weak acidic or neutral condition for the acid−base equilibrium reaction of pyranine.

Acid−Base Equilibria of Other pH Indicator Dyes. If the relationships between pH_{pore} and pH_{bulk} found for pyranine are intrinsic features in the TMAP-HMM system, the evaluated pH_{pore} shown in Figure 3 can predict acid−base equilibria of other pH indicator dyes within TMAP-HMM. From eq 3, pH_{pore} can be written using the fraction of the PyO^- form of pyranine, x_{Py}.

$$pH_{pore} = 7.4 + \alpha + \log\left(\frac{x_{Py}}{1-x_{Py}}\right) \quad (4)$$

Here, since pH indicator dyes with a few sulfonate groups, such as APTS, TPPS, and 2NT, adsorb at the surface TMAP layer by electrostatic interaction, similarly to pyranine, α values of these indicators can be considered to be close to that of pyranine. Accordingly, on the assumption that α values of all pH indicator dyes are the same, the fraction x of base forms of APTS ($PyNH_2$) and 2NT (NpO^-) can be given by substituting eq 4 into eq 3

$$pK_{bulk} - 7.4 = \log\left(\frac{x_{Py}}{1-x_{Py}}\right) - \log\left(\frac{x}{1-x}\right) \quad (5)$$

where pK_{bulk} is the dissociation constant of APTS or 2NT in bulk water. For TPPS, there are two dissociation constants and description of the relationship between fractions of each form and pH_{pore} is difficult. Herein, fraction of a base form ($TPPS^{4-}$) was approximately evaluated using eq 5 and pK_{bulk} of 4.8 (Table 1).

The calculated fractions of base forms of APTS, 2NT, and TPPS are shown in Figure 5, together with the experimental fractions of base forms of these pH indicator dyes measured in bulk water. The details of the estimation of pK_{bulk} values for APTS, 2NT, and TPPS in bulk water are described in

dx.doi.org/10.1021/ac102935q |Anal. Chem. 2011, 83, 2939–2946

Support-
ing Information. Figure 5 predicts that APTS and TPPS within TMAP-HMM are hardly protonated when pH_{bulk} is in the range of 2.1 to 9.1. On the other hand, protonation of 2NT within TMAP-HMM is maintained in the pH_{bulk} range from 2.1 to 9.1. These predictions of acid−base equilibria of pH indicator dyes were further examined by fluorescence experiments.

Figure 6 shows fluorescence excitation spectra of APTS, TPPS, and 2NT within TMAP-HMM, together with normalized fluorescence excitation spectra of these dyes in bulk water at low and high pH_{bulk} values. The absorption and fluorescence excitation spectra of these pH indicator dyes were also measured in bulk water for a series of pH_{bulk} values (Figures S5 to S10, Supporting Information). In the fluorescence excitation spectra of APTS within TMAP-HMM measured at pH_{bulk} values of 2.0, 4.5, and 8.1, a strong band ascribed to the base form of APTS ($PyNH_2$)[25] is observed at ca. 440 nm, but there are no bands ascribed to the acid form of APTS ($PyNH_3^+$) which is known to show structured bands at 384, 369, 349, and 334 nm.[25] The spectral features and fluorescence intensity are independent of pH_{bulk}, indicating that APTS within TMAP-HMM is hardly protonated at pH_{bulk} values of 2.0 to 8.1. In the fluorescence excitation spectra of TPPS within TMAP-HMM observed at pH_{bulk} values of 2.0, 5.6, and 7.5, the spectral shape is similar to the one observed for the base form of TPPS ($TPPS^{4-}$) in bulk water. A strong band at 417 nm and structured bands at 517, 553, and 581 nm can be assigned to the Soret band and Q bands of the base form ($TPPS^{4-}$),[26] respectively. The spectral features and intensity are independent of pH_{bulk}, indicating that the base form ($TPPS^{4-}$) is the major species within TMAP-HMM in the pH_{bulk} range from 2.0 to 7.5. In the fluorescence excitation spectra of 2NT within TMAP-HMM observed at pH_{bulk} values of 2.0, 5.4, and 8.3, all spectral features are similar to those of the acid form of 2NT in bulk solution and there are no remarkable bands corresponding to the base form, indicating that the acid form (NpOH) is the major species within TMAP-HMM in the pH_{bulk} range from 2.0 to 8.3. The acid−base equilibrium reactions experimentally found for APTS, TPPS, and 2NT agree well with those predicted by the effective pH_{pore} inside the TMAP-modified silica mesopore. Therefore, the relationships between pH_{pore} and pH_{bulk} found for pyranine (Figure 4) are intrinsic features in the TMAP-HMM system.

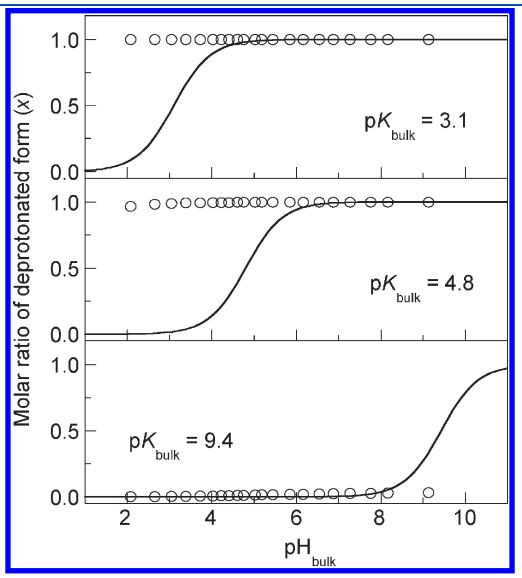

Figure 5. Calculated fractions of deprotonated forms of pH indicator dyes with different pK_{bulk} values (open circles). The solid curves are the fractions of deprotonated forms of pH indicator dyes in bulk water.

In the present study, the relationships between pH_{pore} and pH_{bulk} could be obtained from a simple analysis of fluorescence excitation spectra of pyranine within TMAP-HMM. The relationship between pH_{pore} and pH_{bulk} shown in Figure 4 seems to be similar to that found in sodium bis(2-ethylhexyl) sultosuccinate (AOT) reverse micelles.[15,39,40] For example, Hasegawa[15] studied the relationship between the pH values of aqueous solutions adjusted before solubilization and the local pH of a water nanopool using pH indicator dyes such as pyranine and fluorescein. The results showed that the local pH of the water nanopool was almost constant around 5 even though the pH of the aqueous solution before solubilization was regulated from 2 to 9. Similar experiments on the local pH of a water nanopool were reported in a ^{51}V NMR study using anionic decavanadate oligomer.[40] Results of the present study infer that the shift of pH_{pore} is 1.8 ($\Delta pH_{pore} = 1.8$) for the change in pH_{bulk} from 2.1 to 9.1 ($\Delta pH_{bulk} = 7$). In the AOT reverse micelle system, the water nanopool is surrounded by negatively charged AOT groups,

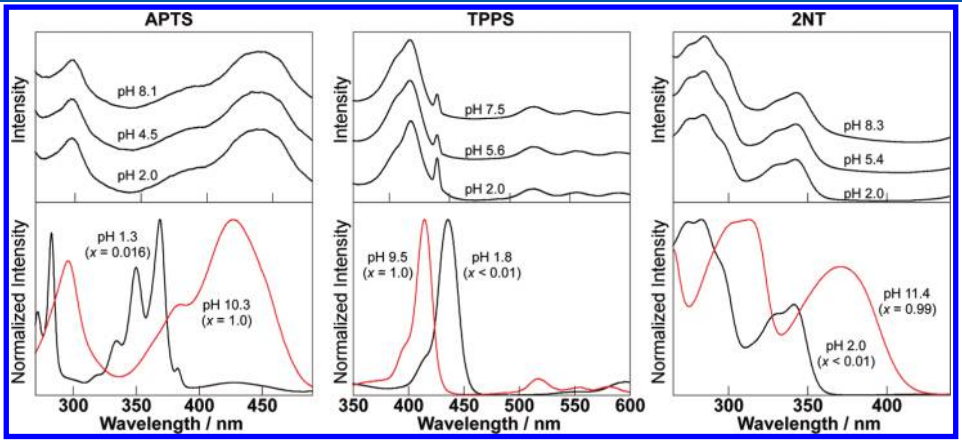

Figure 6. Fluorescence excitation spectra of pH indicator dyes within TMAP-HMM (top row) and in bulk aqueous solution (bottom row) obtained for different solution pH values. Emission wavelength: APTS, 505 nm; TPPS, 660 nm; 2NT, 460 nm. In the bottom row, *x* represents the fraction of the base form of each pH indicator dye.

dx.doi.org/10.1021/ac102935q |*Anal. Chem.* 2011, 83, 2939–2946

and the anionic probes are most likely localized in the central region of the water nanopool owing to electrostatic repulsion between pyranine and AOT.[15,40] This situation is opposite the case of pyranine within TMAP-HMM; pyranine was located in the vicinity of the positively charged surface TMAP layer. The fact that there are similar pH conditions for the AOT reverse micelle and TMAP-HMM systems suggests the possibility that the relationship between pH_{pore} and pH_{bulk} shown in Figure 4 is the intrinsic feature inside the silica mesopore with a positively or negatively charged surface. A more detailed study on pH_{pore} requires that both the p*K* value and the proton concentration inside the silica mesopore are determined separately not only from fluorescence experiments but also by other experimental techniques which have been proven as useful to study the proton concentration in reverse micelles.[39,40]

CONCLUSION

We studied the acid−base equilibria and the effective proton concentration inside the TMAP-modified silica mesopore (silica framework diameter = 3.1 nm) by steady-state fluorescence experiments. Results of the fluorescence experiments showed that the acid−base equilibria of four pH indicator dyes (pyranine, APTS, TPPS, 2NT) within the TMAP-modified silica mesopore were quite different from those in bulk water. From the analysis of the acid−base equilibrium of pyranine, the relationships between pH_{bulk} and the effective proton concentration (pH_{pore}) were obtained as follows: (1) shift of pH_{pore} was 1.8 ($\Delta pH_{pore} = 1.8$) for the pH_{bulk} change from 2.1 to 9.1 ($\Delta pH_{bulk} = 7.0$); (2) pH_{pore} was not simply proportional to pH_{bulk}; (3) the inside of the TMAP-modified silica mesopore was in a weak acidic or neutral condition for the acid−base equilibrium reaction of pyranine when pH_{bulk} ranged from 2.0 to 9.1. Since these relationships between pH_{bulk} and pH_{pore} could explain the acid−base equilibria of other pH indicator dyes (APTS, TPPS, 2NT), it was concluded to be the intrinsic feature for TMAP-modified silica mesopore.

Although the absolute value of pH_{pore} could not be obtained in this study, it could be said that the effective proton concentration inside the TMAP-modified silica mesopore was significantly different from the proton concentration in bulk water. Our results will contribute to promoting the science and technology of inorganic nanoporous materials, since proton concentration is a common interest in the regulation of chemical reactions.

ASSOCIATED CONTENT

Supporting Information. Experimental details for nitrogen adsorption and desorption isotherm, XRD, ^{29}Si CP/MAS NMR, and elemental analysis measurements. Development of eq 2. Time-course adsorption profiles of pH indicator dyes (Figure S1). Nitrogen adsorption isotherms and pore distribution curves of TMAP-HMM and HMM (Figure S2). XRD patterns of TMAP-HMM and HMM and ^{29}Si CP/MAS NMR spectrum for TMAP-HMM (Figure S3). The absorption and fluorescence excitation spectra of pH indicator dyes as a function of solution pH (Figures S4 to S10). The estimation of p*K* values for pH indicator dyes. This material is available free of charge via the Internet at http://pubs.acs.org.

AUTHOR INFORMATION

Corresponding Author

*E-mail: yakira@mx.ibaraki.ac.jp (A.Y.); teramae@m.tains.tohoku.ac.jp (N.T.).

Present Addresses

[⊥]Tsuruoka National College of Technology ,Tsuruoka, Yamagata 997-8511, Japan.

ACKNOWLEDGMENT

This work was supported in part by Grants-in-Aid for Scientific Research (No. 21685009 and No. 22225003) from the Ministry of Education, Culture, Sports, Science and Technology, Japan.

REFERENCES

(1) Sparreboom, W.; van den Berg, A.; Eijkel, J. C. T. *Nat. Nanotechnol.* **2009**, *4*, 713–720.
(2) Brinker, C. J.; Dunphy, D. R. *Curr. Opin. Colloid Interface Sci.* **2006**, *11*, 126–132.
(3) Vinu, A.; Hossain, K. Z.; Ariga, K. *J. Nanosci. Nanotechnol.* **2005**, *5*, 347–371.
(4) Hatton, B.; Landskron, K.; Whitnall, W.; Perovic, D.; Ozin, G. A. *Acc. Chem. Res.* **2005**, *38*, 305–312.
(5) Bartl, M. H.; Boettcher, S. W.; Frindell, K. L.; Stucky, G. D. *Acc. Chem. Res.* **2005**, *38*, 263–271.
(6) Carreon, M. A.; Guliants, V. V. *Eur. J. Inorg. Chem.* **2005**, 27–43.
(7) Soler-Illia, G. J. A. A.; Sanchez, C.; Lebeau, B.; Patarin, J. *Chem. Rev.* **2002**, *102*, 4093–4138.
(8) Martin, C. R.; Kohli, P. *Nat. Rev. Drug Discovery* **2003**, *2*, 29–37.
(9) Cazacu, A.; Legrand, Y.-M.; Pasc, A.; Nasr, G.; van der Lee, A.; Mahon, E.; Barboiu, M. *Proc. Natl. Acad. Sci. U.S.A.* **2009**, *106*, 8117–8122.
(10) Fan, R.; Huh, S.; Yan, R.; Arnold, J.; Yang, P. *Nat. Mater.* **2008**, *7*, 303–307.
(11) Fattakhova-Rohlfing, D.; Wark, M.; Rathousky, J. *Chem. Mater.* **2007**, *19*, 1640–1647.
(12) Newton, M. R.; Bohaty, A. K.; White, H. S.; Zharov, I. *J. Am. Chem. Soc.* **2005**, *127*, 7268–7269.
(13) Gao, Q.; Xu, W.; Xu, Y.; Wu, D.; Sun, Y.; Deng, F.; Shen, W. *J. Phys. Chem. B* **2008**, *112*, 2261–2267.
(14) Rosenholm, J. M.; Czuryszkiewicz, T.; Kleitz, F.; Rosenholm, J. B.; Linden, M. *Langmuir* **2007**, *23*, 4315–4323.
(15) Hasegawa, T. *Langmuir* **2001**, *17*, 1426–1431.
(16) Drummond, C. J.; Grieser, F.; Healy, T. W. *J. Phys. Chem.* **1988**, *92*, 2604–2613.
(17) Fernandez, M. S.; Fromherz, P. *J. Phys. Chem.* **1977**, *81*, 1755–1761.
(18) Tielrooij, K. J.; Cox, M. J.; Bakker, H. J. *ChemPhysChem* **2009**, *10*, 245–251.
(19) Polity, M. J.; Chaimovich, H. *J. Phys. Chem.* **1986**, *90*, 282–287.
(20) Spry, D. B.; Fayer, M. D. *J. Phys. Chem. B* **2009**, *113*, 10210–10221.
(21) Seger, B.; Vinodgopal, K.; Kamat, P. V. *Langmuir* **2007**, *23*, 5471–5476.
(22) Yamaguchi, A.; Uejo, F.; Yoda, T.; Yamashita, T.; Uchida, T.; Tanamura, Y.; Teramae, N. *Nat. Mater.* **2004**, *3*, 337–341.
(23) Yamaguchi, A.; Teramae, N. *Anal. Sci.* **2008**, *24*, 25–30.
(24) Yam, R.; Nachliel, E.; Kiryati, S.; Gutman, M.; Huppert, D. *Biophys. J.* **1991**, *59*, 4–11.
(25) Spry, D. B.; Fayer, M. D. *J. Chem. Phys.* **2008**, *128*, 084508.
(26) Kalyanasundaram, K. *Photochemistry of Polypyridine and Porphyrin Complexes*; Academic Press: London, 1992.
(27) Masad, A.; Huppert, D. *J. Phys. Chem.* **1992**, *96*, 7324–7328.
(28) Smith, K. K.; Kaufmann, K. J.; Huppert, D.; Gutman, M. *Chem. Phys. Lett.* **1979**, *64*, 522–527.
(29) Kamijo, T.; Yamaguchi, A.; Suzuki, S.; Teramae, N.; Itoh, T.; Ikeda, T. *J. Phys. Chem. A* **2008**, *112*, 11535–11542.

(30) Yamaguchi, A.; Watanabe, J.; Mahmoud, M. M.; Fujiwara, R.; Morita, K.; Yamashita, T.; Amino, Y.; Chen., Y.; Radhakrishnan, L.; Teramae, M. *Anal. Chim. Acta* **2006**, *556*, 157–163.
(31) Maria Chong, A. S.; Zhao, X. S. *J. Phys. Chem. B* **2003**, *107*, 12650–12657.
(32) Yuan, P.; Southon, P. D.; Liu, Z.; Green, M. E. R.; Hook, J. M.; Antill, S. J.; Kepert, C. J. *J. Phys. Chem. C* **2008**, *112*, 15742–15751.
(33) Hess, C.; Wild, U.; Schlogl, R. *Microporous Mesoporous Mater.* **2006**, *95*, 339–349.
(34) Yamaguchi, A.; Yoda, T.; Suzuki, S.; Morita, K.; Teramae, N. *Anal. Sci.* **2006**, *21*, 1501–1507.
(35) Liu, Y.-H.; Lin, H.-P.; Mou, C.-Y. *Langmuir* **2004**, *20*, 3231–3239.
(36) Ek, S.; Iiskola, E. I.; Niinisto, L.; Vaittinen, J.; Pakkanen, T. T.; Keranen, J.; Auroux, A. *Langmuir* **2003**, *19*, 10601–10609.
(37) Ramirez, A.; Lopez, B. L.; Sierra, L. *J. Phys. Chem. B* **2003**, *107*, 9275–9280.
(38) Zhao, X. S.; Lu, G. Q.; Whittaker, A. K.; Millar, G. J.; Zhu, H. Y. *J. Phys. Chem. B* **1997**, *101*, 6525–6531.
(39) Fujii, H.; Kawai, T.; Nishikawa, H. *Bull. Chem. Soc. Jpn.* **1979**, *52*, 2051–2055.
(40) Baruah, B.; Roden, J. M.; Sedgwick, M.; Correa, N. M.; Crans, D. C.; Levinger, N. E. *J. Am. Chem. Soc.* **2006**, *128*, 12758–12765.